

---

This is an electronic reprint of the original article.  
This reprint may differ from the original in pagination and typographic detail.

Caro, Miguel A.; Määttä, Jukka; Lopez-Acevedo, Olga; Laurila, Tomi

## Energy band alignment and electronic states of amorphous carbon surfaces in vacuo and in aqueous environment

*Published in:*  
Journal of Applied Physics

*DOI:*  
[10.1063/1.4905915](https://doi.org/10.1063/1.4905915)

Published: 01/01/2015

*Document Version*  
Publisher's PDF, also known as Version of record

*Please cite the original version:*

Caro, M. A., Määttä, J., Lopez-Acevedo, O., & Laurila, T. (2015). Energy band alignment and electronic states of amorphous carbon surfaces in vacuo and in aqueous environment. *Journal of Applied Physics*, 117(3), 034502. <https://doi.org/10.1063/1.4905915>

---

This material is protected by copyright and other intellectual property rights, and duplication or sale of all or part of any of the repository collections is not permitted, except that material may be duplicated by you for your research use or educational purposes in electronic or print form. You must obtain permission for any other use. Electronic or print copies may not be offered, whether for sale or otherwise to anyone who is not an authorised user.

# Energy band alignment and electronic states of amorphous carbon surfaces in vacuo and in aqueous environment

Miguel A. Caro, Jukka Määttä, Olga Lopez-Acevedo, and Tomi Laurila

Citation: *Journal of Applied Physics* **117**, 034502 (2015); doi: 10.1063/1.4905915

View online: <https://doi.org/10.1063/1.4905915>

View Table of Contents: <http://aip.scitation.org/toc/jap/117/3>

Published by the *American Institute of Physics*

---

## Articles you may be interested in

[Density and localized states' impact on amorphous carbon electron transport mechanisms](#)

*Journal of Applied Physics* **120**, 214303 (2016); 10.1063/1.4971010

[Accurate schemes for calculation of thermodynamic properties of liquid mixtures from molecular dynamics simulations](#)

*The Journal of Chemical Physics* **145**, 244504 (2016); 10.1063/1.4973001

[Doping as a means to probe the potential dependence of dopamine adsorption on carbon-based surfaces: A first-principles study](#)

*The Journal of Chemical Physics* **146**, 234704 (2017); 10.1063/1.4986521

[General formulation of pressure and stress tensor for arbitrary many-body interaction potentials under periodic boundary conditions](#)

*The Journal of Chemical Physics* **131**, 154107 (2009); 10.1063/1.3245303

[Hybrid functionals based on a screened Coulomb potential](#)

*The Journal of Chemical Physics* **118**, 8207 (2003); 10.1063/1.1564060

[Structure-property relations in amorphous carbon for photovoltaics](#)

*Applied Physics Letters* **105**, 043903 (2014); 10.1063/1.4891498

---

**AIP** | Journal of Applied Physics

SPECIAL TOPICS



# Energy band alignment and electronic states of amorphous carbon surfaces *in vacuo* and in aqueous environment

Miguel A. Caro,<sup>1,2,a)</sup> Jukka Määttä,<sup>3</sup> Olga Lopez-Acevedo,<sup>2</sup> and Tomi Laurila<sup>1</sup>

<sup>1</sup>Department of Electrical Engineering and Automation, Aalto University, Espoo, Finland

<sup>2</sup>Department of Applied Physics, COMP Centre of Excellence in Computational Nanoscience, Aalto University, Espoo, Finland

<sup>3</sup>Department of Chemistry, Aalto University, Espoo, Finland

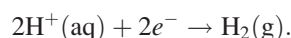
(Received 17 October 2014; accepted 1 January 2015; published online 15 January 2015)

In this paper, we obtain the energy band positions of amorphous carbon (a-C) surfaces in vacuum and in aqueous environment. The calculations are performed using a combination of (i) classical molecular dynamics (MD), (ii) Kohn-Sham density functional theory with the Perdew-Burke-Ernzerhof (PBE) exchange-correlation functional, and (iii) the screened-exchange hybrid functional of Heyd, Scuseria, and Ernzerhof (HSE). PBE allows an accurate generation of a-C and the evaluation of the local electrostatic potential in the a-C/water system, HSE yields an improved description of energetic positions which is critical in this case, and classical MD enables a computationally affordable description of water. Our explicit calculation shows that, both *in vacuo* and in aqueous environment, the a-C electronic states available in the region comprised between the H<sub>2</sub>/H<sub>2</sub>O and O<sub>2</sub>/H<sub>2</sub>O levels of water correspond to both occupied and unoccupied states within the a-C pseudogap region. These are localized states associated to *sp*<sup>2</sup> sites in a-C. The band realignment induces a shift of approximately 300 meV of the a-C energy band positions with respect to the redox levels of water. © 2015 AIP Publishing LLC.

[<http://dx.doi.org/10.1063/1.4905915>]

## I. INTRODUCTION

The use of amorphous carbon (a-C) and tetrahedral amorphous carbon (ta-C) as electrode coating for electrochemical detection of organic molecules has gathered widespread attention in recent years. Amorphous carbon offers ideal properties for *in vivo* and *in vitro* applications: chemical inertness, biocompatibility, corrosion and bacterial resistance, and CMOS integrability.<sup>1–3</sup> A property of central interest for any electrode material is the position of its energy bands within the electrochemical scale. This scale is typically defined with respect to the standard hydrogen electrode (SHE), which marks the reduction reaction potential of a proton pair in aqueous solution to form hydrogen gas



The absolute potential of the SHE is around 4.43 V below the vacuum level.<sup>4</sup> The position of a material's energy bands within this scale is critical because it determines the energy regions in which the material presents available electronic states, which can then be exploited to favor specific redox reactions.

The matter of determining energy band positions accurately is far from trivial. The most widely used theoretical frame to deal with the interaction between electrons and nuclei at the quantum level, Kohn-Sham density functional theory (DFT),<sup>5,6</sup> presents fundamental limitations with regard to band gap prediction.<sup>7–9</sup> In order to overcome this limitation of the standard Kohn-Sham formalism, so-called

generalized Kohn-Sham approaches have been proposed.<sup>10</sup>

A more accurate description and better agreement with experiment is achieved in these generalized schemes at the expense of a much higher computational cost. Since performing calculations at this level of theory is not always realistically affordable, ingenious strategies are needed to overcome these limitations. In this paper, we calculate the absolute position of the electronic states of a-C surfaces in vacuum and in an aqueous environment using a combination of different levels of theory: classical molecular dynamics (MD), Kohn-Sham DFT, and screened-exchange hybrid-functional DFT.<sup>11</sup>

## II. SIMULATION DETAILS AND RESULTS

### A. a-C surface *in vacuo*

The computational generation of the a-C surface was done following the approach described in detail in our recent work.<sup>12</sup> The system is constructed with a hydrogen passivation layer at the bottom and allowing the structure to relax following a conjugated-gradient minimization of the total DFT energy, using the Perdew-Burke-Ernzerhof (PBE) parametrization of the gradient-corrected exchange-correlation energy functional.<sup>13</sup> An appropriate amount of vacuum is added on top to prevent interaction with periodic replicas of the structure and to ensure the vacuum level is converged to the correct energy value. In order to correct for the spurious macroscopic polarization arising from finite-size effects, dipole corrections along the direction perpendicular to the plane of the surface are applied.<sup>14,15</sup> Since we have previously observed little correlation between Fermi level

<sup>a)</sup>Electronic mail: mcaroba@gmail.com

position and a-C sample density,<sup>12</sup> the chosen sample in this work is the 3.03 g/cm<sup>3</sup> sample from Ref. 12, whose density is around that of ta-C, most interesting in the context of electrode coating. After the system's geometry is obtained in the PBE-DFT frame, a static self-consistent calculation is performed for fixed atomic positions using the screened-exchange hybrid-functional approach of Heyd, Scuseria, and Ernzerhof (HSE).<sup>11</sup> The latter allows an accurate evaluation of the position of the different single-particle eigenvalues. In particular, the distance between the eigenvalue corresponding to the highest occupied single-particle state and the lowest unoccupied one is associated with the band gap in semiconductors and insulators and is severely underestimated in standard DFT approximations, including PBE-DFT.<sup>7,8</sup> The calculations at both PBE-DFT and HSE-DFT levels of theory were performed in the context of the projector augmented-wave (PAW)<sup>16,17</sup> method as implemented in the VASP code.<sup>18,19</sup> More details on how the calculations were carried out can be found in Ref. 12. The electronic density of states (DOS) and local Hartree potential of the structure are shown in Fig. 1, where the most significant features are (i) the prediction of a true (although very narrow) bandgap by the HSE functional in contrast to its absence from the PBE calculation, (ii) the corresponding shift

downwards of valence states and upward of conduction states, and (iii) the prediction by the HSE calculation of a vacuum level only  $\sim 84$  meV above that predicted by PBE, when referenced to the a-C surface's average Hartree potential. Note that the vacuum level shifts at around  $z = 30$  Å in Fig. 1 due to the applied dipole correction and the periodic boundary conditions. What this shift signifies is a different work function for the different sides of the a-C slab. We are interested in the value for the upper side which is the a-C surface (the lower side is the H passivation layer). In this context, we conclude that the PBE level of theory is sufficient to obtain the value of the vacuum level but not to get the energy band positions, or to predict the existence of a true bandgap for that matter. This so-called "bandgap problem" of Kohn-Sham DFT<sup>7,8</sup> is, together with the existence of dangling bonds in a-C,<sup>20</sup> responsible for the presence of the peak at  $E_F$  for the PBE DOS calculation. A more detailed discussion on the estimation of the bandgap of a-C and the existence of dangling bonds will be presented in Appendix A. As will be shown later on, the HSE bandgap widens in the bulk a-C case while it remains not present for the PBE functional. We can refer the vacuum level from the HSE calculation to the a-C surface's average Hartree potential

$$E_{\text{vacuum}} - E_{\text{Hartree}}^{\text{a-C}} \approx 13.08 \text{ eV}. \quad (1)$$

Note that the number above is only valid for the current sample with density 3.03 g/cm<sup>3</sup>. We will use  $E_{\text{Hartree}}^{\text{a-C}}$  alone as a common reference for the electronic DOS of equivalent structures: the surface *in vacuo* and the exact same surface in aqueous environment. In practice, this removes the uncertainty associated to determining a universal value of  $E_{\text{vacuum}} - E_{\text{Hartree}}^{\text{a-C}}$ . Also, note the difference in Eq. (1) cannot be extrapolated to the aqueous case because of the shift in the absolute position  $E_{\text{Hartree}}^{\text{a-C}}$  when water molecules are in contact with the surface. This shift cannot be easily estimated without an explicit calculation including a-C, water and vacuum.

## B. a-C surface in aqueous environment

When an a-C/water interface is present, the electric dipoles created due to the redistribution of electric charge affect the position of the electronic states with respect to the vacuum case previously studied. For the calculation of the position of the a-C electronic states within the electrochemical scale, we resort to a variant of the method proposed by Wu *et al.* for semiconductors.<sup>21</sup> This is based on the idea of using electrostatic potentials as local reference energy levels in the different material layers that make up the system. This method, mixed with different levels of theory for computing the band positions, has been successfully employed to study for instance semiconductor heterojunctions.<sup>22,23</sup> The idea in this case is to refer the electronic states of bulk a-C and the H<sub>2</sub>/H<sub>2</sub>O level of bulk water to their respective average Hartree potentials in the interfacial a-C/water system. Within this approach, the calculation is carried out in a three-step process which avoids the use of simulation cells that would be too large to be manageable by an *ab initio* method. In

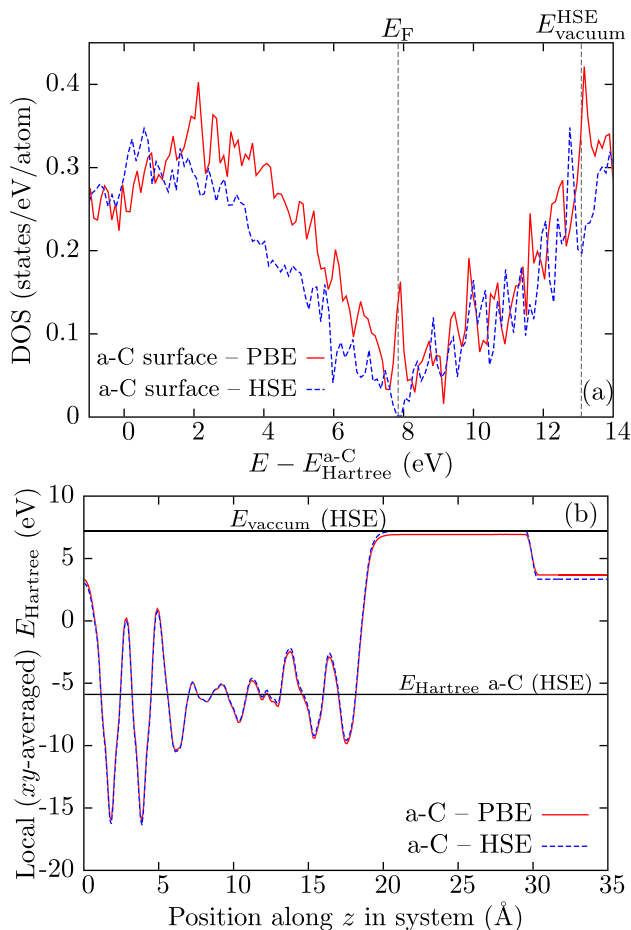


FIG. 1. (a) Electronic density of states of the a-C surface sample in vacuum used in this work, calculated using the PBE and HSE functionals as described throughout the text. (b) Local Hartree potential (in-plane average) along the direction perpendicular to the a-C surface.

TABLE I. Levels of theory used to study the different properties of a-C and water isolated subsystems, and the interfacial a-C/water system.

a-C surface <i>in vacuo</i>		a-C surface in aqueous environment	
		a-C	Water
Atomic	PBE	PBE (kept fixed)	TIP4P (water/water); Lennard-Jones (water/a-C)
Electronic	HSE (PBE for comparison)	PBE (electrostatic potential, a-C + H <sub>2</sub> O system);	HSE (electronic DOS, band positions)

contrast to Ref. 21, which relied on the conventional PBE-DFT approach to calculate the position of conduction band edges, we use the HSE-DFT approach to ensure an accurate determination of the energetic positions of the a-C electronic states. The need for a hybrid-type or equivalent approach in order to accurately determine these positions was already highlighted in that work. While Ref. 21 assigns the H<sub>2</sub>/H<sub>2</sub>O level to an empty state introduced by a H<sub>3</sub>O<sup>+</sup> molecule, the correct way to calculate the position of this level is by computing the change in Gibbs free energy of the H<sub>2</sub> production process with a hydrated proton H<sup>+</sup> (or H<sub>3</sub>O<sup>+</sup> molecule) and a free electron as starting system. This procedure, in the context of DFT, has been presented by Lucking *et al.* in a recent paper.<sup>24</sup> This method avoids the explicit use of the Kohn-Sham eigenvalues of water and relies on the electrostatic energy instead, which is accurately computed within DFT. Recent studies show that in order to correctly compute the band positions of water one must resort to a scheme beyond DFT (e.g., hybrid-type or many-body perturbation theory), for which large system calculations are prohibitive.<sup>25,26</sup> Table I presents a summary of the different levels of theory used to treat the different parts of the system at each step. The details are described in the following.

The first step following Wu's methodology<sup>21</sup> would be to compute the position of the electronic states of bulk a-C with respect to its average Hartree potential. However, as we have previously discussed in Sec. II A,  $E_{\text{vacuum}} - E_{\text{Hartree}}^{\text{a-C}}$  may change with sample's density. For a reconstructed a-C surface, there is a local drop in density as one moves away from the bulk-like region towards the surface/vacuum interface.<sup>12</sup> This means that  $E_{\text{Hartree}}^{\text{a-C}}$  lies at different levels for bulk and surface samples, and cannot be used as a common reference. In Fig. 2(a), we show the electronic DOS for a bulk sample generated at the PBE-DFT level of theory as explained in Ref. 12. A static self-consistent HSE-DFT calculation is carried out to obtain the position of the single-particle states. The HSE results for the DOS in the energy gap region, together with a comparison with the results from a PBE calculation, are shown in the figure. The determination of the optical gap following the Tauc procedure,<sup>27</sup> described in detail in Appendix A, yields  $E_{\text{g}}^{\text{Tauc}} = 1.3$  eV, in good agreement with recent tight-binding results by Mathioudakis *et al.*<sup>28</sup> It can be clearly observed how the DOS profile of the bulk sample is shifted upward by over 500 meV compared to the DOS profile of the surface structure shown in Fig. 1(a). One way to work around this issue would be to compute the progressive change in  $E_{\text{vacuum}} - E_{\text{Hartree}}^{\text{a-C}}$  for a very large surface structure as the system size is increased. This is unrealistic from the computational point of view given that the sample size we are dealing with is

already quite expensive to generate. Another way to solve the problem is to use the electronic structure of the surface system directly, rather than the bulk one, since obviously the reference average electrostatic potential in the a-C region does not change in that case. We have opted for this second strategy.

The justification for using the electronic structure of the surface arises from the fact that both bulk and surface have the same general structure with only variations in the density of states around the gap. In particular, the position of the Fermi level (understood as the energy value half way between conduction and valence band edges) and the position of the  $sp^3$ -related diamond-like states that delimit the pseudogap do not show correlation with  $sp^2$  fraction.<sup>12,29</sup> Therefore, while  $sp^2$ -related states within the pseudogap vary between surface and bulk systems,  $sp^3$ -related states are common to both systems. In Fig. 2(b), we show the

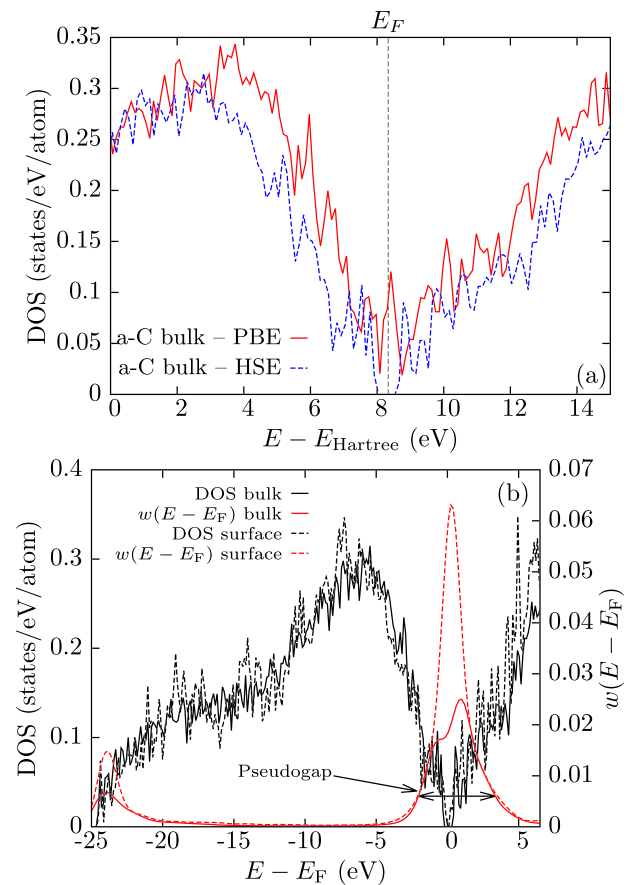


FIG. 2. (a) Electronic DOS for the same bulk a-C sample of density 3.03 g/cm<sup>3</sup>, obtained with the PBE and HSE functionals. (b) Localization of electronic states in the different energy regions for bulk [Fig. 2(a)] and surface [Fig. 1(a)] systems, obtained with the HSE functional.

localization of electronic states in surface and bulk systems using the localization function  $w(E - E_F)$  proposed by Tritsarlis *et al.*,<sup>30</sup> which is defined in terms of the projected DOS

$$w(E) = \sum_{\alpha=1}^N \frac{(Ng_{\alpha}(E)/g(E) - 1)^2}{N(N-1)}, \quad (2)$$

where the sum runs over the  $N$  atoms in the sample,  $E$  is the energy level, and  $g(E)$  and  $g_{\alpha}(E)$  are the total and partial DOS, respectively. Further comment on the use of this function for the analysis of the present a-C networks can be found in Ref. 12. The figure allows a direct comparison between the localization in both surface and bulk cases, which can be observed to be very similar and share their peak center position. A definition of where the pseudogap lies is to some extent arbitrary, but should rely on localization properties, such as the mobility edge. Here, we have defined the pseudogap to lie in the energy region for which the localization function  $w(E - E_F)$  rises above 0.006. This allows an unambiguous definition of pseudogap which turns out to be about the same for surface and bulk systems. This value has been chosen so that the width of the pseudogap is approximately the same as the band gap of diamond (5.43 eV using the HSE functional<sup>31</sup>). The expression that references the electronic DOS of a-C to the  $H_2/H_2O$  level then becomes

$$E_{\text{DOS}}^{\text{a-C}} - E_{H_2/H_2O} = \underbrace{E_{\text{DOS}}^{\text{a-C,surf}} - E_{\text{Hartree}}^{\text{a-C,surf}}}_{\text{step 1}} + \underbrace{E_{\text{Hartree}}^{\text{water}} - E_{H_2/H_2O}}_{\text{step 2}} + \underbrace{E_{\text{Hartree}}^{\text{a-C,surf}} - E_{\text{Hartree}}^{\text{water}}}_{\text{step 3}}, \quad (3)$$

where the quantities calculated in each step are noted explicitly, and  $E_{\text{DOS}}^{\text{a-C,surf}}$  has substituted the  $E_{\text{DOS}}^{\text{a-C,bulk}}$  from Ref. 21. Steps 2 and 3 will be described in the following. This three step method is validated for the a-C/water system in Appendix B.

The second step is the calculation of the position of the  $H_2/H_2O$  and  $O_2/H_2O$  levels of water. In order to do so, we still assume that  $E_{H_2/H_2O} - E_{\text{Hartree}}^{\text{water}}$  remains the same as for bulk water, as proposed by Wu *et al.*,<sup>21</sup> but obtain its value from the related quantities calculated by Lucking *et al.*<sup>24</sup> and the water redox potentials known experimentally. Lucking *et al.* calculated the average Hartree potential of water to lie 2.97 eV below the vacuum level, whereas the  $H_2/H_2O$  level lies 4.43 eV below vacuum<sup>4</sup> and the  $O_2/H_2O$  level lies 1.23 eV below that,<sup>32</sup> therefore 5.66 eV below vacuum. Thus, the offsets for the  $H_2/H_2O$  and  $O_2/H_2O$  levels with respect to the average Hartree potential of water are

$$\begin{aligned} E_{H_2/H_2O} - E_{\text{Hartree}}^{\text{water}} &= -1.46 \text{ eV}, \\ E_{O_2/H_2O} - E_{\text{Hartree}}^{\text{water}} &= -2.69 \text{ eV}. \end{aligned} \quad (4)$$

The third and final step consists in the explicit interface calculation, where the a-C surface and the water molecules are contained in the same supercell. In addition, vacuum needs to be included in order to be able to apply dipole corrections to compensate for the spurious macroscopic dipole

introduced by the interface due to finite size-effects and the differing work functions in the upper and lower sides of the a-C slab. This dipole leads to a linearly varying potential in the water layer, as will be shown later. The full system under study is depicted in Fig. 3.

As pointed out on a series of papers on DFT modeling of water,<sup>33–35</sup> DFT does not necessarily provide an improved structural description of water if compared to accurate classical potentials. The authors suggest performing classical MD of water using the TIP4P potential,<sup>36</sup> which provides a good description of the bulk properties of water, in order to determine its atomic structure. Then, a DFT calculation is carried out for fixed atomic positions to obtain electronic properties. Recently, Pham *et al.*<sup>25</sup> have shown that different potentials used for the modeling of water give electrostatic potentials in good agreement with each other, further supporting the validity of the procedure. We follow this approach. In this case, the atoms in the a-C surface are kept fixed and the water molecules around it are equilibrated for 100 ps during a classical MD simulation. The classical MD run is performed in the NVT ensemble at 298 K for a periodic

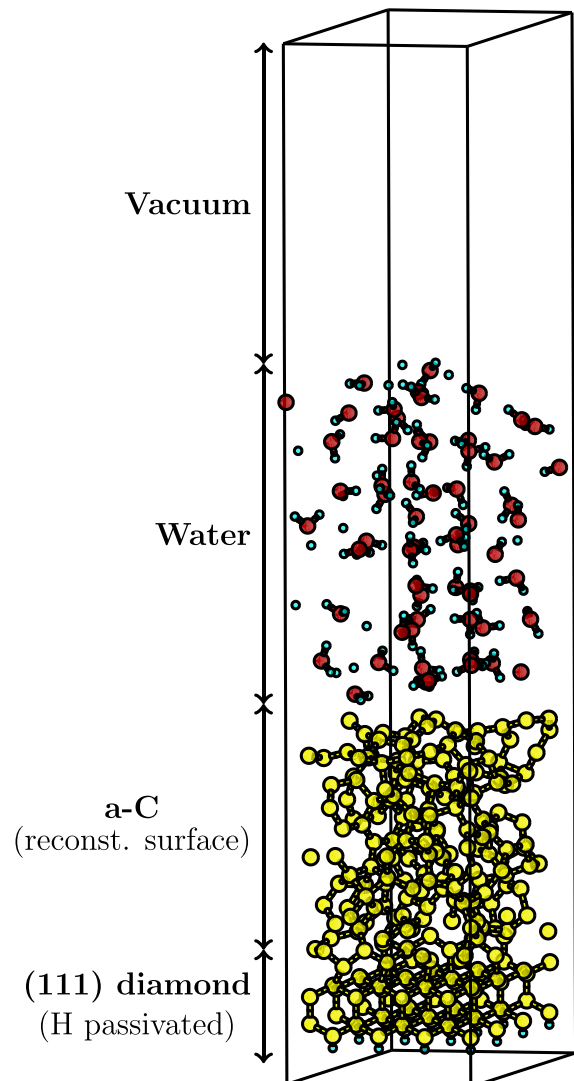


FIG. 3. a-C + water + vacuum system used to study the offset in average Hartree potentials between a-C and water.

supercell containing the a-C structure and 60 water molecules with the GROMACS suite.<sup>37,38</sup>

Although ideally NTP conditions would be used, in the case of a solid/liquid interface these are unfeasible since in classical MD pressure is handled via a constant compressibility parameter for the whole simulation box, which varies greatly between solids and liquids. We assume a-C as incompressible compared to water. However, there is some vacuum in the simulation box so that the water molecules can relax along the  $z$  direction (perpendicular to the surface plane) to compensate the pressure frustrations. This allows conditions similar to NTP for water relaxation. For the a-C atoms, the rigid treatment generates less errors than dynamics using classical harmonic bonds. Bond lengths are often restrained with LINCS<sup>39</sup> in classical MD. Compared to hydrogens in hydrated a-C interfaces, the pure carbon atoms of the hydrophobic a-C used here are very heavy and are expected to move less: the water molecules will reorient instead. Therefore, the static conditions for the a-C atoms are reasonable. Similar NVT conditions with rigid interface have previously been used in studying the interfacial behavior of water on graphene and silica substrates.<sup>40–42</sup>

The interactions between water molecules are described with the TIP4P potential and the interactions between a-C and water are modeled via Lennard-Jones potentials, using the GROMACS implementation of the CHARMM force field.<sup>43</sup> The local Hartree potential calculated at the PBE level of theory is shown in Fig. 4, for 16 snapshots at 5 ps intervals of the same MD trajectory. It can be observed that the local Hartree potential is characteristic of the different layers that make up the system: on the left-hand side a regular profile that corresponds to the H-passivated diamond substrate, then an irregular profile for the a-C layer followed by another irregular profile for the H<sub>2</sub>O molecules that varies between snapshots (the average potential in the water region does not vary significantly), and finally the flat vacuum potential. Note that without dipole correction an incorrect linearly decreasing average potential would have been obtained for water.

For periodic structures, there exist “nanosmoothing” techniques to obtain the average Hartree potential away from interfaces.<sup>44,45</sup> In the present case, we are dealing with an amorphous solid (a-C) and an irregular liquid (water), which in practice limits the applicability of these techniques. We therefore obtain  $E_{\text{Hartree}}^{\text{a-C}}$  as an average within the a-C region of the supercell. Since this average is computed in the same way as for the a-C surface in vacuum, any *absolute* error is removed by adding and subtracting this value [Eq. (3)]. For water, we note that the computed average  $E_{\text{Hartree}}^{\text{water}}$  varies very little between different snapshots of the MD run, and the trajectory-averaged value can therefore be used as a solid reference energy. The difference in average Hartree potential between the a-C and water regions is indicated in the figure, and amounts to

$$\Delta E_{\text{Hartree}} = 9.82 \text{ eV}.$$

As we have already discussed, the number above is not a universal value for a-C but serves as a reference for the alignment of electronic states if the same surface structure is used to calculate both quantities.

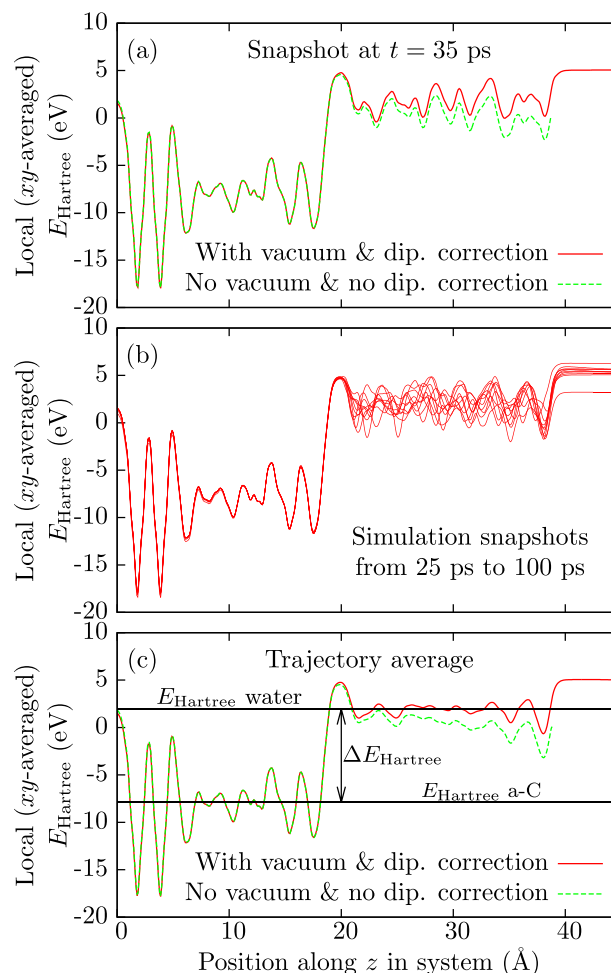


FIG. 4. Local Hartree potential of the a-C/water interface plotted along the direction perpendicular to the a-C surface. (a) Individual snapshot, (b) different snapshots at 5 ps intervals from  $t = 25$  ps to  $t = 100$  ps, and (c) trajectory averages.

### III. DISCUSSION AND CONCLUSIONS

The main results of this paper are presented and summarized in Fig. 5. Fig. 5(a) shows the electronic DOS of the a-C surface in vacuum, referred to the vacuum level. The experimental values of the H<sub>2</sub>/H<sub>2</sub>O and O<sub>2</sub>/H<sub>2</sub>O levels are given, for reference, with respect to the vacuum level for a-C obtained in this work. Fig. 5(b) shows the position of the electronic DOS of a-C in aqueous environment with respect to the redox levels of water, referred to the electrochemical scale, which takes its origin at the SHE. The electronic states of a-C are shifted upward due the energy band realignment by approximately 300 meV. In this case the redox potentials of water have been explicitly calculated and are given with respect to the average Hartree potential of water in contact with an a-C surface.

The positions of the redox potentials of water in Fig. 5(a) have not been explicitly calculated and are given only for reference. The situation for the a-C surface in contact with water, on the other hand, offers itself to a direct analysis of the DOS distribution with respect to the redox levels of water because those levels have been explicitly calculated within a consistent theoretical frame. The results in Fig. 5(b) show that the electronic states available between the H<sub>2</sub>/H<sub>2</sub>O

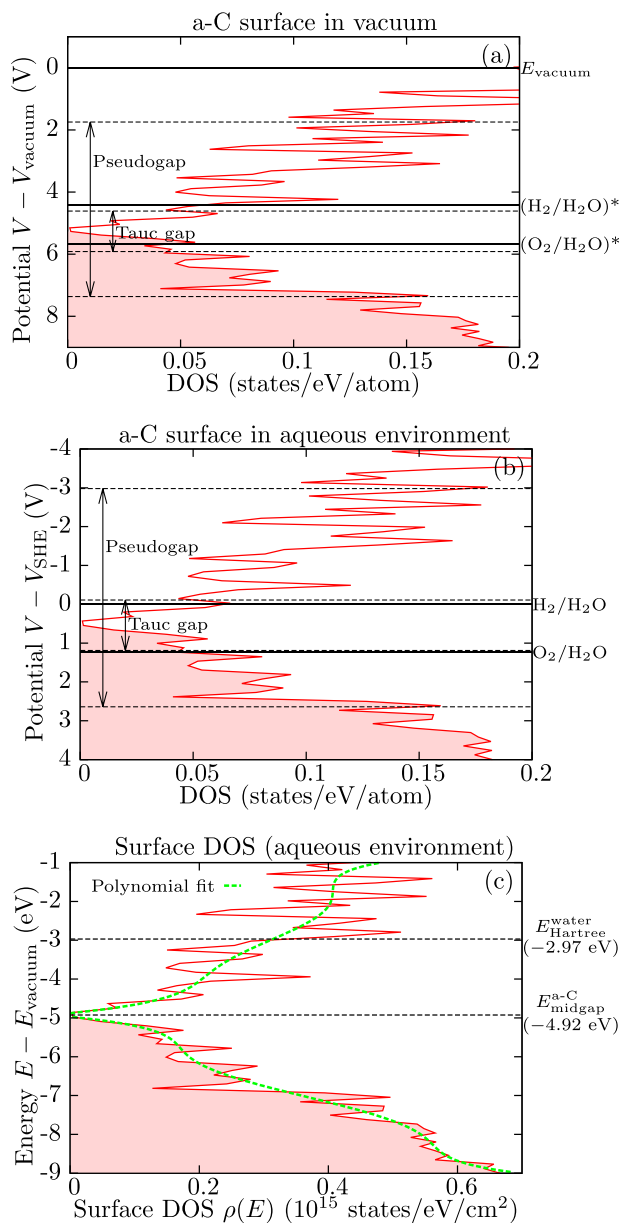


FIG. 5. Electronic density of states distribution of (a) an a-C surface *in vacuo* and (b) a-C in contact with water, where the DOS position with respect to the redox levels of water is calculated explicitly. The redox potentials in (a) are not calculated but taken from experiment and referenced to the vacuum level. Shaded areas indicate occupied states. (c) Surface density of states calculated as explained throughout the text.

and  $O_2/H_2O$  levels of water in direct contact with the a-C surface belong to the pseudogap region of a-C, and encompass the a-C Fermi level, corresponding approximately to the optical (Tauc) gap region of a-C. These states tend to be localized and related to  $sp^2$  sites, which are more abundant right at the very surface of the material and whose number and delocalized character increases for lower a-C sample's density.<sup>12</sup> It is therefore to be expected that a higher number of states becomes available as the density of the a-C used for electrode coating decreases.

In outer-sphere electrochemical reactions, the reactant and product do not interact strongly with the electrode's surface. Thus, they are not specifically adsorbed and generally stay at a distance of at least a solvent layer from the

electrode, i.e., at the outer Helmholtz plane. In such cases the density of states calculated here has immediate applicability. This is because contrary to inner-sphere electrode reactions, such as hydrogen or oxygen evolution, which involve considerable reorganization of the solvation shell and specific adsorption, outer-sphere redox systems are almost exclusively characterized by the electronic structure of the analyte compounds. Within the Gerischer-Marcus formalism,<sup>46-49</sup> the reaction rate constants for reduction and oxidation of a redox couple O/R are

$$k_f = \frac{1}{\Delta t} \int_{-\infty}^{\infty} \varepsilon_{\text{red}}(E, \Delta t) W_O(\lambda, E) f(E) \rho(E) dE, \quad (5)$$

for the reduction of O, and

$$k_b = \frac{1}{\Delta t} \int_{-\infty}^{\infty} \varepsilon_{\text{ox}}(E, \Delta t) W_R(\lambda, E) [1 - f(E)] \rho(E) dE, \quad (6)$$

for the oxidation of R.  $\Delta t$  is a time step short enough to ensure that the electronic properties of surface and analyte solution do not change significantly and  $\varepsilon_{\text{red/ox}}(E, \Delta t)$  is the probability of the reduction/oxidation taking place in the interval  $\Delta t$ , normalized by the concentration of O/R species. Therefore,  $\varepsilon_{\text{red/ox}}(E, \Delta t)/\Delta t$  is a probability per unit time which for sufficiently small  $\Delta t$  should be independent of the latter.  $W_{O/R}(\lambda, E)$  is a probability density for the O/R species. Finally,  $f(E)$  is Fermi's distribution function and  $\rho(E)$  is a surface density of states. The parameter  $\lambda$ , called *reorganization energy*, characterizes the energetic separation between the energy levels at which the oxidation and reduction reactions occur and their spread: in the case of symmetric concentration distributions, for instance given as Gaussians in Marcus theory, the center of the distribution  $W_O(\lambda, E)$  and the center of  $W_R(\lambda, E)$  are separated by  $2\lambda$ , and the distribution's standard deviation is given by  $\sigma = \sqrt{2\lambda kT}$ , where  $k$  is the Boltzmann constant and  $T$  is the temperature.<sup>46,49</sup>

In a simple model, the center position of  $W_O(\lambda, E)$  is given by the lowest unoccupied molecular orbital (LUMO) of O, and  $W_R(\lambda, E)$  is given by the highest occupied molecular orbital (HOMO) of R. Therefore,  $\varepsilon_{\text{red}}(E, \Delta t)/\Delta t$  and  $\varepsilon_{\text{ox}}(E, \Delta t)/\Delta t$  account for the probabilities per unit time of filling the LUMO of O and emptying the HOMO of R, respectively. The effect of varying the electrode's potential is achieved through the shift in the Fermi level and the corresponding change in the distribution function  $f(E)$

$$f(E) = \frac{1}{1 + \exp[(E - E_F)/kT]}. \quad (7)$$

$\varepsilon_{\text{red/ox}}(E, \Delta t)/\Delta t$  can be estimated for instance following Fermi's golden rule from overlap integrals of the orbitals,<sup>50</sup> and possibly from more sophisticated schemes, such as time-dependent DFT. These quantities are analyte-specific and a detailed study lies beyond the scope of the present paper. Future work will aim at exhaustive characterization of the interaction between a-C and different analytes.

The surface's density of states  $\rho(E)$  can be directly estimated from the DOS profiles of Fig. 5 as a simple multiplication by the number of atoms per unit area. We used the AREAIMOL tool<sup>51</sup> from the CCP4 suite<sup>52</sup> to calculate the number of surface atoms based on the “rolling ball” algorithm.<sup>53</sup> Using a probe sphere of 0.75 Å, which corresponds to approximately half of the first nearest-neighbor distance (position of the first peak in the radial distribution function),<sup>12</sup> yields 29 surface atoms in our simulation cell, consistent with an intuitive visual inspection of Fig. 3, equivalent to  $3.11 \times 10^{15}$  atoms/cm<sup>2</sup>. Multiplying this number by the DOS gives an estimate of the number of electronic states per eV and cm<sup>2</sup> available at the a-C surface. A suitable approximation for  $\rho(E)$  valid within the energy range of Fig. 5(c) can be provided as a 5th degree polynomial

$$\rho(E) \approx \begin{cases} -0.0153E^5 - 0.537E^4 - 7.47E^3 - 51.3E^2 \\ -174E - 235 & \text{for } E < -4.92 \text{ eV} \\ 0.0129E^5 + 0.185E^4 + 1.02E^3 + 2.61E^2 \\ +3.18E + 1.89 & \text{for } E > -4.92 \text{ eV,} \end{cases} \quad (8)$$

which is given in units of  $10^{15}$  states/eV/cm<sup>2</sup> and valid for  $E$  in eV and referenced to the vacuum level. The surface density of states and the polynomial approximation are displayed in Fig. 5(c).

The main consequences of the reduced number of states in the pseudogap region, immediately evident from Eqs. (5) and (6), are a wider water window, an increased overpotential and slower electron transfer kinetics for a-C electrochemistry compared to the use of metal electrodes, where the density of states remains high and relatively constant in the energy region of interest. This expected behavior ties in with the experimental findings.<sup>3,54</sup> In addition, the observations that the density of functional groups (-COOH and -OH, for instance) is low in a-C surfaces<sup>54</sup> and the surface reactivity, e.g., towards dopamine,<sup>2</sup> is not significantly altered by different oxidation treatments underlines the fact that the available density of states remains approximately the same as for pure a-C surfaces. Further computational work from our group will now focus on describing the interaction of specific outer-sphere analytes with a-C electrodes, building up from the work presented in this article.

## ACKNOWLEDGMENTS

Computational resources were provided by Aalto University's Science-IT project through the Triton cluster, and by CSC-IT Center for Science through the Taito cluster. M.A.C. would like to thank Tuan Anh Pham from UC Davis and Daniel Opalka from Cambridge University for helpful comments on the modeling of acceptor and donor levels in water. The authors acknowledge financial support from the Finnish National Agency for Technology and Innovation (Grant No. 211488) and the Academy of Finland through its Centres of Excellence Program (Project No. 251748). J.M. acknowledges the financial support of the Marie Curie Career Integration Grants within the seventh European Community Framework Programme through Grant No. 293861.

## APPENDIX A: ELECTRONIC STRUCTURE AND BANDGAP DETERMINATION FOR a-C

### 1. Electronic structure

The existence of the “bandgap problem” in Kohn-Sham DFT<sup>7,8</sup> affects the determination of the electronic structure of both surface and bulk samples studied in this work at the PBE level. In particular, PBE and other local and semilocal functionals lead to the general quantitative underestimation of energy gaps in insulators and semiconductors. In the present case, it also leads to the incorrect qualitative prediction of the absence of a band gap in our a-C structures. A striking feature for instance is the appearance of a marked peak at the Fermi level in both bulk and surface DOS which is absent from the HSE DOS in Figs. 1(a) and 2(a). For our 192-atom simulation cell (bulk sample), the peak at the Fermi level arises from two unpaired  $sp^2$  atoms as seen in Fig. 6 (top). In the figure, yellow atoms are  $sp^3$  coordinated and orange atoms are  $sp^2$  coordinated. The unpaired atoms are isolated  $sp^2$  sites and are marked in red. Two defects in a 192-atom cell with density  $\sim 3$  g/cm<sup>3</sup> correspond to a defect density of  $\sim 1.5 \times 10^{21}$  cm<sup>-3</sup>, which is in agreement with reported electron spin resonance data.<sup>20,55</sup> This peak is inherited by the surface structure which is constructed from the bulk.<sup>12</sup> Note that, experimentally, some of these dangling bonds will

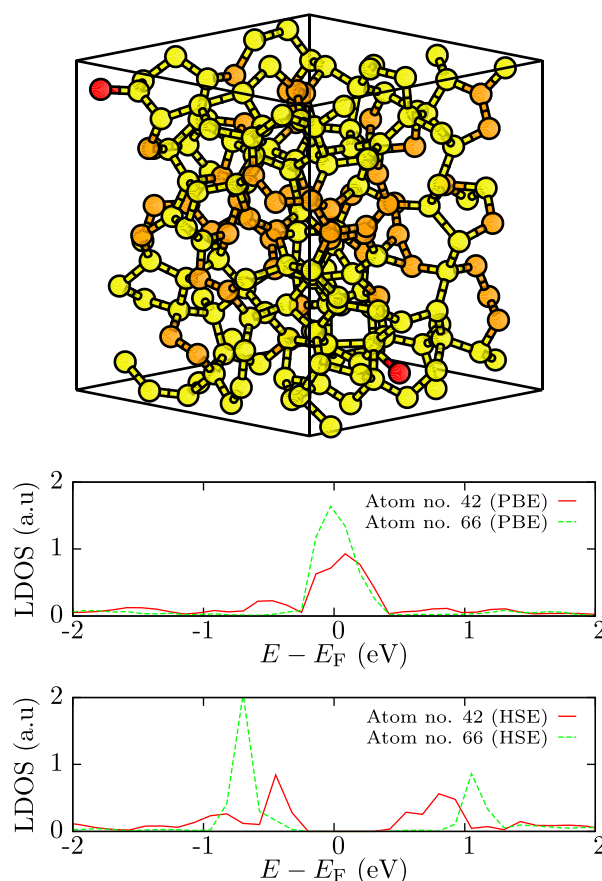


FIG. 6. (Top) Atomic network for the a-C bulk sample used in the present study. (Bottom) Local DOS (LDOS) for the dangling bond sites in the bulk a-C sample.

eventually be saturated by unintentional hydrogen incorporation. This can be expected from the much lower spin density observed in hydrogenated a-C.<sup>20</sup> The peak position at the Fermi level is incorrect and not observed in experiment, and is a spurious result introduced by the DFT “bandgap problem.” This peak does not disappear from the HSE calculation; however, the separation between the  $\pi$  and  $\pi^*$  orbitals increases, giving the impression that the peak disappears, as can be observed in Fig. 6 (bottom). The figure shows the projected DOS on the two sites colored in red in Fig. 6 (top) at both PBE and HSE levels of theory. As can be observed, the peak does not disappear but the HSE functional manages to correctly describe the separation between  $\pi$  and  $\pi^*$  orbitals thus clearing these states from the gap.

The discussion above serves to illustrate the challenges of accurate modeling of energy gaps from *ab initio* quantum mechanical calculations, in particular for narrow gap materials, and to justify the scheme employed in this work, where PBE is used to generate the structure and HSE to get the correct energetic ordering of the orbitals. In the present case, the wrong energetic positioning of  $\sigma$  and  $\sigma^*$  states in a-C is “pushing” the  $\pi$  and  $\pi^*$  states close to each other. Thus, a spurious narrowing of about 2 eV in the  $\sigma$ - $\sigma^*$  gap coming from the PBE functional, which can be inferred from the DOS profile in Fig. 2(a) by comparing it to the HSE DOS, leads to a corresponding reduction of the  $\pi$ - $\pi^*$  gap through the interaction between  $\sigma$  and  $\pi$  orbitals. The extreme consequence of this is that  $\pi$  and  $\pi^*$  states closest to the Fermi level overlap at  $E_F$  when computed using the PBE functional.

## 2. Bandgap determination: Tauc approach

Even without the fundamental issues related to DFT, the determination of bandgap in amorphous materials is already problematic. This is due to the existence of both localized and extended states, and the different optical transitions that can take place between them, as discussed in detail by Knief and von Niessen regarding the determination of the optical gap of amorphous Si (a-Si).<sup>56</sup> The authors argue that a Tauc plot is the most suitable method to compare computational and experimental gaps, and the Tauc approach is indeed commonly used to compute the bandgap of a-C.<sup>1,28</sup> While the Tauc gap might be useful at high  $sp^3$  fractions, for low  $sp^3$  fractions the similarities between a-C and a-Si are less pronounced and the suitability of the Tauc approach is reduced. Early on, Dasgupta *et al.* already questioned the suitability of the procedure for a-C.<sup>20</sup> Since we are in a relatively high  $sp^3$  fraction regime, the Tauc approach should however be reasonably reliable and in any case useful for further characterization of our a-C sample. The Tauc gap is determined from the onset of linear absorption, obtained as the intersection of a linear fit to the absorption curve in the region where it behaves linearly.<sup>27</sup> Computationally, it can be obtained for instance from the evolution of the square root of the joint density of states (JDOS) as a function of photon energy  $\hbar\omega$ ,<sup>56,57</sup> as seen in Fig. 7. The value we extract from the HSE calculation, 1.3 eV, is in good

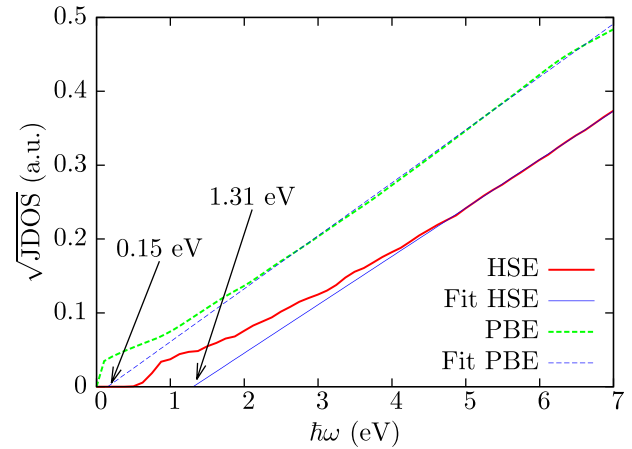


FIG. 7. Tauc gap determined with the JDOS technique for the present bulk a-C sample.

agreement with the recent tight-binding results of Mathioudakis *et al.*<sup>28</sup> As expected, the PBE calculation severely underestimates this value.

## APPENDIX B: VALIDATION OF THE THREE-STEP METHOD

In order to probe the validity of Eq. (3), we propose a “direct versus indirect” comparison of the position of the low-lying  $s$ -like semicore levels of oxygen with respect to the Fermi level of a-C. The direct calculation uses the

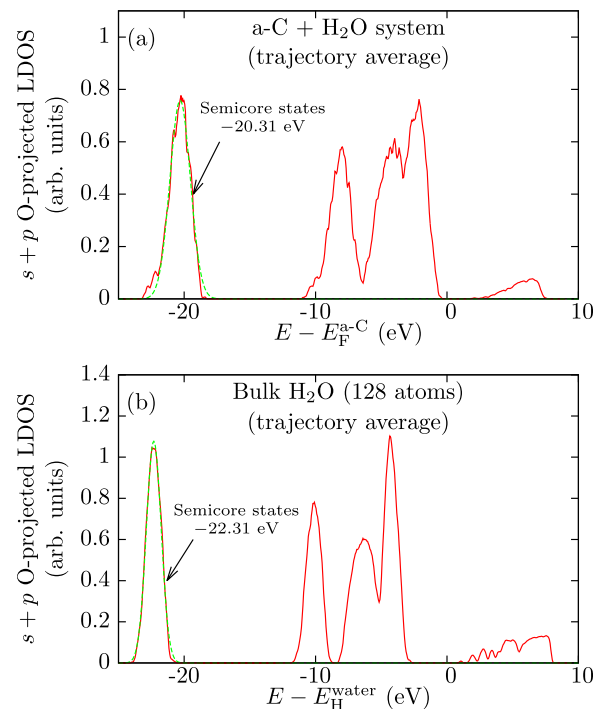


FIG. 8. LDOS (combined  $s + p$  orbital components) projected onto the O atoms belonging to water molecules in (a) the a-C/water system and (b) bulk water. Both results are MD trajectory averages for 16 snapshots at 5 ps intervals between  $t = 25$  ps and  $t = 100$  ps. Indicated are the  $s$ -like semicore levels of O and their peak-center position on the graph, with green-dashed lines showing the Gaussian fit employed.

peak-center position of these levels, using a Gaussian fit, for the MD trajectory average in the explicit interfacial system, as shown in Fig. 8(a). This value is simply

$$(E_F^{a-C} - E_{\text{semicore}}^{\text{water}})_{\text{direct}} = 20.31 \text{ eV.} \quad (\text{B1})$$

The indirect calculation involves the use of Eq. (3)

$$\begin{aligned} (E_F^{a-C} - E_{\text{semicore}}^{\text{water}})_{\text{indirect}} &= (E_F^{a-C} - E_H^{a-C})_{\text{surface}} + (E_H^{\text{water}} - E_{\text{semicore}}^{\text{water}})_{\text{bulk}} \\ &\quad + (E_H^{a-C} - E_H^{\text{water}})_{\text{interface}}. \end{aligned} \quad (\text{B2})$$

$E_F^{a-C} - E_H^{a-C}$  is obtained from the a-C surface in vacuum (Fig. 1) and amounts to 7.84 eV;  $E_H^{\text{water}} - E_{\text{semicore}}^{\text{water}}$  is obtained from a bulk water calculation [Fig. 8(b)] and equals 22.31 eV; finally,  $E_H^{a-C} - E_H^{\text{water}}$  is obtained from the explicit a-C/water interface calculation [Fig. 4(c)] and, as we have shown at the end of Sec. II B, its value in the present example is  $-9.82$  eV. Their sum is 20.33 eV, which is in excellent agreement with the direct result, thus supporting the validity of the three-step method, Eq. (3).

- <sup>1</sup>J. Robertson, *Mater. Sci. Eng., R* **37**, 129 (2002).
- <sup>2</sup>T. Laurila, A. Rautiainen, S. Sintonen, H. Jiang, E. Kaivosoja, and J. Koskinen, *Mater. Sci. Eng., C* **34**, 446 (2014).
- <sup>3</sup>E. Kaivosoja, S. Sainio, J. Lyytinen, T. Palomäki, T. Laurila, S. I. Kim, J. G. Han, and J. Koskinen, *Surf. Coat. Technol.* **259**, 33 (2014).
- <sup>4</sup>H. Reiss and A. Heller, *J. Phys. Chem.* **89**, 4207 (1985).
- <sup>5</sup>P. Hohenberg and W. Kohn, *Phys. Rev.* **136**, B864 (1964).
- <sup>6</sup>W. Kohn and L. J. Sham, *Phys. Rev.* **140**, A1133 (1965).
- <sup>7</sup>J. P. Perdew and M. Levy, *Phys. Rev. Lett.* **51**, 1884 (1983).
- <sup>8</sup>L. J. Sham and M. Schlüter, *Phys. Rev. Lett.* **51**, 1888 (1983).
- <sup>9</sup>L. J. Sham and M. Schlüter, *Phys. Rev. B* **32**, 3883 (1985).
- <sup>10</sup>A. Seidl, A. Görling, P. Vogl, J. A. Majewski, and M. Levy, *Phys. Rev. B* **53**, 3764 (1996).
- <sup>11</sup>J. Heyd, G. E. Scuseria, and M. Ernzerhof, *J. Chem. Phys.* **118**, 8207 (2003).
- <sup>12</sup>M. A. Caro, R. Zoubkoff, O. Lopez-Acevedo, and T. Laurila, *Carbon* **77**, 1168 (2014).
- <sup>13</sup>J. P. Perdew, K. Burke, and M. Ernzerhof, *Phys. Rev. Lett.* **77**, 3865 (1996).
- <sup>14</sup>J. Neugebauer and M. Scheffler, *Phys. Rev. B* **46**, 16067 (1992).
- <sup>15</sup>G. Makov and M. C. Payne, *Phys. Rev. B* **51**, 4014 (1995).
- <sup>16</sup>P. E. Blöchl, *Phys. Rev. B* **50**, 17953 (1994).
- <sup>17</sup>G. Kresse and D. Joubert, *Phys. Rev. B* **59**, 1758 (1999).
- <sup>18</sup>G. Kresse and J. Furthmüller, *Phys. Rev. B* **54**, 11169 (1996).
- <sup>19</sup>See <http://www.vasp.at> for Vienna Ab initio Simulation Package (VASP).
- <sup>20</sup>D. Dasgupta, F. Demichelis, C. F. Pirri, and A. Tagliaferro, *Phys. Rev. B* **43**, 2131 (1991).
- <sup>21</sup>Y. Wu, M. K. Y. Chan, and G. Ceder, *Phys. Rev. B* **83**, 235301 (2011).
- <sup>22</sup>C. G. Van de Walle and R. M. Martin, *Phys. Rev. B* **34**, 5621 (1986).
- <sup>23</sup>S. B. Zhang, D. Tománek, S. G. Louie, M. L. Cohen, and M. S. Hybertsen, *Solid State Commun.* **66**, 585 (1988).
- <sup>24</sup>M. Lucking, Y.-Y. Sun, D. West, and S. Zhang, *Chem. Sci.* **5**, 1216 (2014).
- <sup>25</sup>T. A. Pham, C. Zhang, E. Schwegler, and G. Galli, *Phys. Rev. B* **89**, 060202 (2014).
- <sup>26</sup>D. Opalka, T. A. Pham, M. Sprik, and G. Galli, *J. Chem. Phys.* **141**, 034501 (2014).
- <sup>27</sup>J. Tauc, R. Grigorovici, and A. Vancu, *Phys. Status Solidi B* **15**, 627 (1966).
- <sup>28</sup>C. Mathioudakis, G. Kopidakis, P. Patsalas, and P. C. Kelires, *Diamond Relat. Mater.* **16**, 1788 (2007).
- <sup>29</sup>A. Ilie, A. Hart, A. J. Flewitt, J. Robertson, and W. I. Milne, *J. Appl. Phys.* **88**, 6002 (2000).
- <sup>30</sup>G. A. Tritsarlis, C. Mathioudakis, P. C. Kelires, and E. Kaxiras, *J. Appl. Phys.* **112**, 103503 (2012).
- <sup>31</sup>J. Heyd and G. E. Scuseria, *J. Chem. Phys.* **121**, 1187 (2004).
- <sup>32</sup>H. D. Gesser, *Applied Chemistry: A Textbook for Engineers and Technologists* (Springer, 2002).
- <sup>33</sup>J. C. Grossman, E. Schwegler, E. W. Draeger, F. Gygi, and G. Galli, *J. Chem. Phys.* **120**, 300 (2004).
- <sup>34</sup>E. Schwegler, J. C. Grossman, F. Gygi, and G. Galli, *J. Chem. Phys.* **121**, 5400 (2004).
- <sup>35</sup>D. Prendergast, J. C. Grossman, and G. Galli, *J. Chem. Phys.* **123**, 014501 (2005).
- <sup>36</sup>W. L. Jorgensen, J. Chandrasekhar, J. D. Madura, R. W. Impey, and M. L. Klein, *J. Chem. Phys.* **79**, 926 (1983).
- <sup>37</sup>D. van der Spoel, E. Lindahl, B. Hess, G. Groenhof, A. E. Mark, and H. J. C. Berendsen, *J. Comput. Chem.* **26**, 1701 (2005).
- <sup>38</sup>B. Hess, C. Kutzner, D. van der Spoel, and E. Lindahl, *J. Chem. Theory Comput.* **4**, 435 (2008).
- <sup>39</sup>B. Hess, H. Bekker, H. J. C. Berendsen, and J. G. E. M. Fraaije, *J. Comput. Chem.* **18**, 1463 (1997).
- <sup>40</sup>D. Argyris, N. R. Tummala, A. Striolo, and D. R. Cole, *J. Phys. Chem. C* **112**, 13587 (2008).
- <sup>41</sup>P. Gallo, M. A. Ricci, and M. Rovere, *J. Chem. Phys.* **116**, 342 (2002).
- <sup>42</sup>M. C. Gordillo and J. Martí, *J. Chem. Phys.* **117**, 3425 (2002).
- <sup>43</sup>P. Bjelkmar, P. Larsson, M. A. Cuendet, B. Hess, and E. Lindahl, *J. Chem. Theory Comput.* **6**, 459 (2010).
- <sup>44</sup>J. Junquera, M. H. Cohen, and K. M. Rabe, *J. Phys.: Condens. Matter* **19**, 213203 (2007).
- <sup>45</sup>M. Mrovec, J.-M. Albina, B. Meyer, and C. Elsässer, *Phys. Rev. B* **79**, 245121 (2009).
- <sup>46</sup>A. J. Bard and L. R. Faulkner, *Electrochemical Methods: Fundamentals and Applications*, 2nd ed. (Wiley, New York, 2001).
- <sup>47</sup>H. Gerischer, *Adv. Electrochem. Electrochem. Eng.* **1**, 139 (1961).
- <sup>48</sup>H. Gerischer, *Physical Chemistry: An Advanced Treatise* (Academic, New York, 1970).
- <sup>49</sup>R. A. Marcus and N. Sutin, *Biochim. Biophys. Acta, Rev. Bioenerg.* **811**, 265 (1985).
- <sup>50</sup>W. J. Royea, A. M. Fajardo, and N. S. Lewis, *J. Phys. Chem. B* **101**, 11152 (1997).
- <sup>51</sup>E. B. Saff and A. B. J. Kuijlaars, *Math. Intell.* **19**, 5 (1997).
- <sup>52</sup>M. D. Winn, C. C. Ballard, K. D. Cowtan, E. J. Dodson, P. Emsley, P. R. Evans, R. M. Keegan, E. B. Krissinel, A. G. W. Leslie, A. McCoy *et al.*, *Acta Crystallogr., Sect. D: Biol. Crystallogr.* **67**, 235 (2011).
- <sup>53</sup>B. Lee and F. M. Richards, *J. Mol. Biol.* **55**, 379 (1971).
- <sup>54</sup>T. Laurila, V. Protopopova, S. Rhode, S. Sainio, T. Palomäki, M. Moram, J. M. Feliu, and J. Koskinen, *Diamond Relat. Mater.* **49**, 62 (2014).
- <sup>55</sup>K. M. Krishna, H. Ebisu, K. Hagimoto, Y. Hayashi, T. Soga, T. Jimbo, and M. Umeno, *Appl. Phys. Lett.* **78**, 294 (2001).
- <sup>56</sup>S. Knief and W. von Niessen, *Phys. Rev. B* **59**, 12940 (1999).
- <sup>57</sup>S. K. O'Leary, S. R. Johnson, and P. K. Lim, *J. Appl. Phys.* **82**, 3334 (1997).